Engineered Nanopore of Phi29 DNA-Packaging Motor for Real-Time Detection of Single Colon Cancer Specific Antibody in Serum

Shaoying Wang,[†,‡] Farzin Haque,[†,‡] Piotr G. Rychahou,[§] B. Mark Evers,[§] and Peixuan Guo[†,‡,§,*]

[†]Nanobiotechnology Center, [‡]Department of Pharmaceutical Sciences, College of Pharmacy, and [§]Markey Cancer Center, University of Kentucky, Lexington, Kentucky 40536, United States

ABSTRACT The ingenious design of the bacterial virus phi29 DNA packaging nanomotor with an elegant and elaborate channel has inspired its application for single molecule detection of antigen/antibody interactions. The hub of this bacterial virus nanomotor is a truncated cone-shaped connector consisting of 12 protein subunits. These subunits form a ring with a central 3.6-nm channel acting as a path for dsDNA to enter during packaging and to exit during infection. The connector has been inserted into a lipid bilayer. Herein, we reengineered an Epithelial Cell Adhesion Molecule (EpCAM) peptide into the C-terminal of nanopore as a probe to specifically detect EpCAM antibody (Ab) in nanomolar concentration at the single molecule level. The binding of Abs sequentially to each peptide probe induced stepwise blocks in current. The distinctive current signatures enabled us to analyze the docking and undocking kinetics of Ab—probe interactions and determine the K_d. The signal of EpCAM antibody can be discriminated from the background events in the presence of nonspecific antibody or serum. Our results demonstrate the feasibility of generating a highly sensitive platform for detecting antibodies at extremely low concentrations in the presence of contaminants.

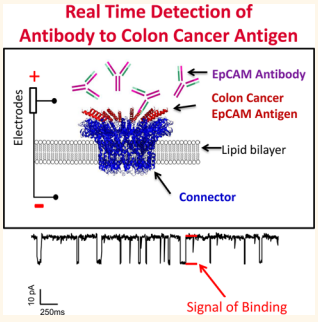

KEYWORDS: nanotechnology · DNA packaging · nanomotor · bacteriophage phi29 · nanopore antibody · EpCAM · single molecule sensing

In biological systems, transmembrane and biomotor channels play critical roles in all aspects of life, such as regulating the traffic of macromolecules and ions into and out of nuclei, organelles, and cells; segregating chromosomes; and translocating and transporting single- or double-stranded DNA.[1−5] In bacterial virus phi29, with the aid of an ATP-driven motor, double-stranded DNA (dsDNA) viruses package their genome into preformed protein shells called procapsids.[6,7] The motor consists of the protein enzyme gp16, which functions as a part of ATPase, six copies of packaging RNA (pRNA),[8−11] and a central protein core called a connector.[12,13] The connector is composed of 12 protein subunits that encircle to form a dodecameric channel, which enables dsDNA to translocate into the procapsid of the phage and exit during maturation and infection.[6−9] The crystal structure of the phi29 connector was determined at atomic resolution.[13] The ring is 13.8 nm at its wide end and 6.6 nm at its narrow end. The internal channel is 6 nm in diameter at the wide end and 3.6 nm in diameter at the narrow end (Figure 1C−E). The wider end (C-terminal) of the connector is located within the capsid, while the narrow end (N-terminal) partially protrudes out of the capsid.

Recently, the connector channel has been incorporated into lipid bilayers to serve as a membrane-embedded nanopore with robust properties. This system has shown sensitive and unique conductance signatures when DNA or ions pass through the channel.[14,15] The channel conductance was uniform, as demonstrated by a perfectly correlated linear response to applied voltage. The connector channel is stable under a wide range of solution conditions, including a pH range of 2 to 12 and different salt species and concentrations.[15] A one-way traffic property for dsDNA translocation from the N-terminal to the C-terminal with a

* Address correspondence to peixuan.guo@uky.edu.

Received for review June 30, 2013 and accepted October 23, 2013.

Published online October 23, 2013
10.1021/nn404435v

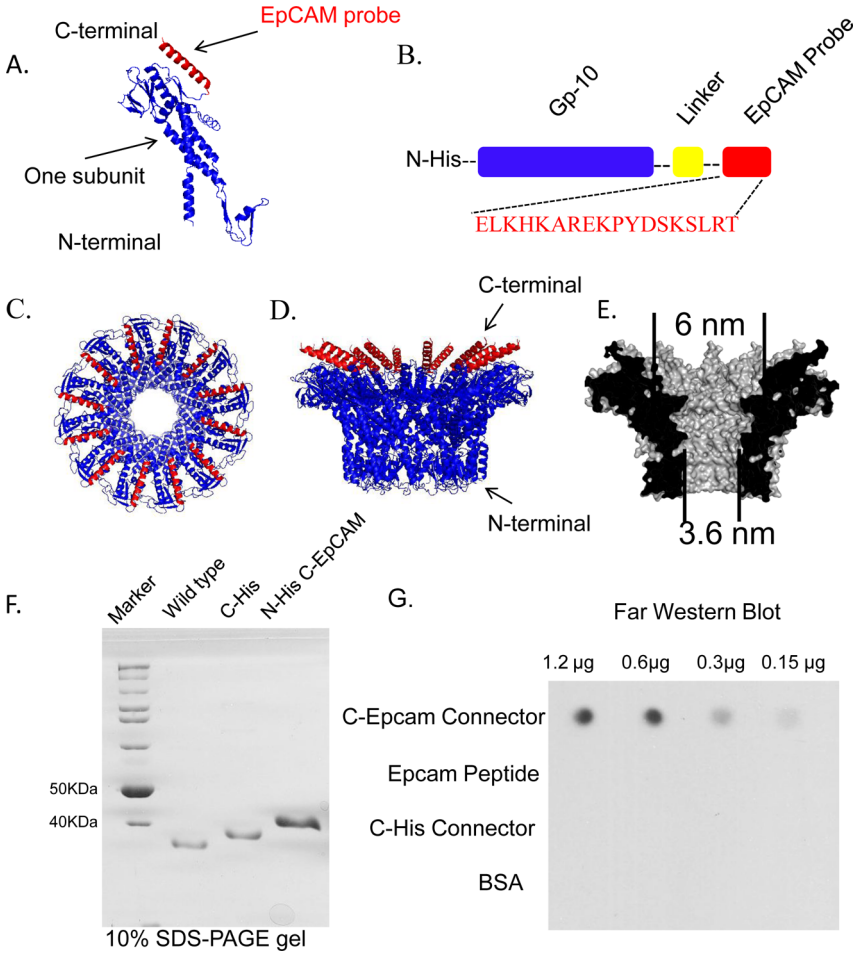

Figure 1. Illustration of the phi29 connector channel structure; (A) structure of one subunit showing the location of the EpCAM probe (red); (B) construction of the modified gp10 gene by insertion of His tag at the N-terminus, 6-Gly linker and EpCAM probe at the C-terminus; (C) top view; (D) side view; and (E) section view of the phi29 connector showing the size of the channel and location of the EpCAM probe (red) incorporated into the phi29 DNA packaging motor channel; (F) molecular weight of wild-type, C-His and N-His C-EpCAM connector on 10% SDS-PAGE; (G) demonstration of the accessibility and specificity of EpCAM probe in the C-terminal of the phi29 connector channel by Far Western blot.

valve mechanism for DNA packaging has also been observed.[16] The connector channel has shown three discrete steps, gating at higher trans-membrane potentials associated with conformational change in the channel subunits.[17] The availability of the crystal structure of this connector channel has enabled explicit engineering with atomic precision for added functionality. Recently, a reengineered connector channel with a reduced channel size has shown the capability to discriminate single-strand DNA or RNA from double strand.[18] By selectively functionalizing a probe in the interior of the channel, we can identify single chemicals with reactive thioesters or maleimide groups based on their distinct fingerprints.[19] Procedures for large-scale production and purification of the connector have already been developed.[14,20−24] Taken together, these features make the connector channel an ideal system for sensing and diagnostic applications.

Nanopore-based sensory techniques have been extensively studied for the detection of a variety of biomacromolecules and chemicals based on modulations of the individual current blockage events.[25−30] Engineered transmembrane channels with various probes are capable of stochastic detection by observing (in real time) the individual binding events between single ligands and receptors with high selectivity and sensitivity.[31−33] The unique current signatures and characteristic binding can reveal the identity and concentration of the target analyte.[34,35] Moreover, the dynamic interaction between the analyte and the probes can be studied in real-time at high resolution by using single channel conduction assays. One advantage of the single molecule techniques is the low limit of detection, which is ideal for the early detection of biomarkers that exist in ultra-low concentrations, making it possible to diagnose specific diseases at an earlier (*i.e.*, asymptomatic) stage.

In this study, we introduced an Epithelial Cell Adhesion Molecule peptide (EpCAM) that was 18 amino acids long as a probe into the C-terminal of each subunit (Figure 1A,B). EpCAM is a cell surface molecule known to be overexpressed by the majority of human

epithelial carcinomas, including prostate, breast, colorectal and head and neck cancers.[36−42] We incorporated this reengineered channel into a lipid bilayer and characterized its conductance properties. We then detected the binding of EpCAM antibody at a single molecule level in nanomolar concentrations based on the unique current signatures. The docking and undocking kinetics of antibody-probe interactions enabled us to determine the K_d. To further test the detection capability of this engineered phi29 channel and push nanopore techniques for clinical utilization, we performed the EpCAM antibody detection in the presence of either nonspecific antibody or diluted serum. We showed that the EpCAM antibody can be distinguished from the background events that are present. Our results demonstrate the feasibility of reengineering the connector channels with a wide range of probes for medical diagnostic applications.

RESULTS

Incorporation of the EpCAM Peptide to the C-terminal End of the Connector. To facilitate connector purification, an N-terminal His tag was inserted just upstream of the gp-10 connector gene. An EpCAM peptide (18 amino acids in length) was inserted downstream of the gp-10 connector channel gene at the C-terminal end. To provide end flexibility, a linker with 6 glycines was included between the gp-10 connector and the EpCAM peptide probe (Figure 1A,B). The reengineered connectors were purified to homogeneity and run on an SDS-PAGE gel (Figure 1F) with wild-type and C-His tagged connectors as controls. The molecular weights of C-His tagged and N-His-C-EpCAM modified connector subunits were 36.7 and 40.6 kDa, respectively. After purification, the reengineered channels with the EpCAM probe assembled into a ring composed of 12 evenly spaced probes in the same plane within the dodecameric connector channel. In addition, we compared the conductance of EpCAM connector channels and C-his connector channels under the same buffer conditions. The similar conductance and histogram distribution that was noted indicates they have similar cross-sectional areas. The accessibility and specificity of EpCAM probes on the engineered connector was further verified by Western blot assays (Figure 1G). Compared with the controls (EpCAM peptide, C-His connector and bovine serum albumin [BSA]), the EpCAM antibody was observed to bind specifically to the EpCAM reengineered connector. The intensity of the band corresponding to EpCAM Ab/EpCAM connector complex increased as the amount of EpCAM engineered connector channel was increased from 0.15 to 1.2 μg (Figure 1G).

Characterization of the Membrane-Embedded EpCAM Reengineered Connector Channels. The EpCAM engineered connector channel was incorporated into planar lipid membranes in two steps, as previously described.[14] The first step was to incorporate the connector into liposomes, followed by insertion into planar lipid membranes *via* vesicle fusion of liposome/connector complexes, to form a membrane-embedded nanopore.[14,15] The insertion of the EpCAM engineered connector channels generated a stepwise increase of the current, as shown in the continuous current trace (Figure 2A). The insertion of EpCAM probe at the C-terminus did not affect the membrane signal stability, voltage gating properties, membrane durability, or the membrane insertion efficiency of the connector channel. The current step size of the EpCAM engineered connector channels was homogeneous (Figure 2C), and the channels showed equal conductance under both positive and negative transmembrane voltages. The average current jump was 55 ± 6 pA (0.74 ± 0.09 nS) in 0.2 M NaCl, 1 mM HEPES, pH 7.4. Conductance was derived at specific, constant holding potentials (+75 or −75 mV) after the phi29 connector channel was incorporated into a lipid membrane and was calculated as the ratio of the current jump induced by a discrete step to the applied voltage. Occasionally, two connector channels were observed to insert simultaneously, as demonstrated by a conductance of 1.43 ± 0.03 nS (Figure 2C). Under the same buffer

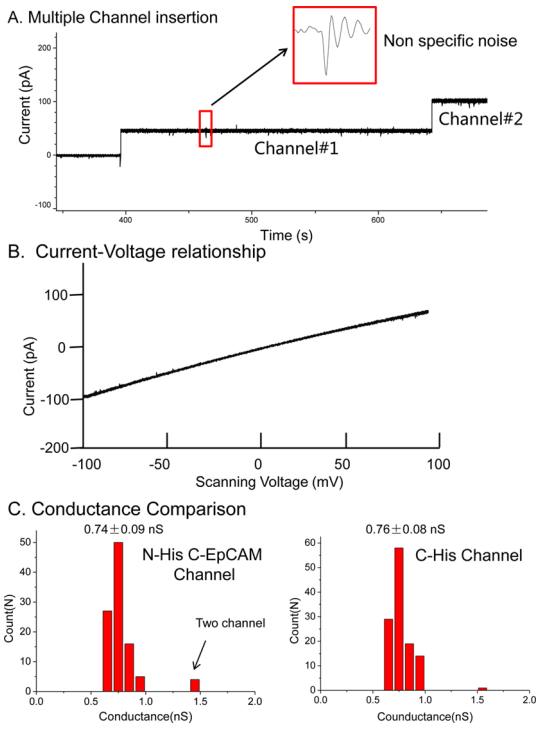

Figure 2. Characterization of membrane-embedded EpCAM engineered phi29 connector channels: (A) continuous current trace showing multiple insertions of EpCAM reengineered connector channels into planar lipid bilayer; (B) current voltage trace under a ramping voltage of −100 to 100 mV; (C) conductance comparison of N-his C-EpCAM and C-his connector channel under the same buffer condition and 75 mV voltage.

condition, the reengineered N-his C-EpCAM connector channel showed similar conductance as C-his connectors (0.76 ± 0.08 nS), indicating that the modification did not change the conductance and size of the channel (Figure 2C). The uniformity of this engineered connector channel was further demonstrated by applying ramping voltage, which showed a nearly linear *I*−*V* relationship without exhibiting any voltage gating phenomenon under the reported conditions of ±100 mV (Figure 2B).

Real-Time Sensing of EpCAM Antibody Interactions with EpCAM Reengineered Connector Channels. Under 0.2 M NaCl, 1 mM HEPES, pH 7.4 buffer solution, series of blocking events were observed in the presence of EpCAM antibody in the cis-chamber. The binding of an EpCAM antibody to each probe induced stepwise blocks (every block represented a single molecule binding) in current (Figure 3B,C), with a corresponding decrease in conductance because of the physical blocking of the channel. One parameter used to characterize the binding events was the current blockage percentage, which represents the difference between the open connector channel and the current after EpCAM antibody binding. Current blockage percentage was calculated as follows: size of current blockage resulting from binding one EpCAM antibody to one connector channel divided by step size of the current for one connector insertion.

Two classes of current blockage signals were observed. The first class represented transient binding events, which may be induced by the temporary and reversible binding of an EpCAM antibody with the probe, shown as recoverable blockage signals (Figure 3B). The second class was the permanent binding events (Figure 3C), which represented tight binding between the EpCAM probe on the connector and the antibody. This second class was observed as discrete stepwise augmentation of current blockage. Both classes of blockage events resulted in ~20 pA reduction in current, which corresponds to 36.8 ± 1.8% for transient events and 34.7 ± 2.6% for permanent binding events (Figure 4A,B). The current blockage was not caused by the translocation of antibody, because the molecular weight of antibody, about 150 kDa, was too large to pass through the connector channel (487 kDa). In addition, given the dimensions of an antibody (14.2 nm × 8.5 nm × 3.8 nm),[43] it is highly unlikely to translocate through the 3.6 nm connector channel.

Another parameter to characterize the antibody and probe interaction is the dwell time (τ), which is the duration of a blockage event. The transient events, on average, had a dwell time of ~30 ms, implying that the transient events are indeed caused by the temporary binding of the EpCAM antibody to the probe on the connector, rather than the unlikely event of translocation through the pore. The dwell time distribution can be used to determine the docking and undocking kinetics of antibody-probe interactions. The binding time of the antibody to the probe is defined as τ_{off}, whereas the duration time between two consecutive blockage events is defined as τ_{on}. Figure 5 represents a statistical analysis of the binding kinetics based on more than 1000 transient binding events. The histograms of τ_{on} and τ_{off} were fitted with a single-exponential distribution function $\exp(\tau/\vec{\tau})$, where $F\vec{\tau}$ is the time constant indicating the association and dissociation processes (Figure 5A,B). The frequencies of association ($1/\vec{\tau}_{on}$) and dissociation ($\vec{\tau}_{off}$) are shown as a function of antibody concentration [*P*] (Figure 5C,D). The association rate constant (k_{on}) was determined using the eq $(1/\vec{\tau}_{on}) = k_{on} \times [P]$.

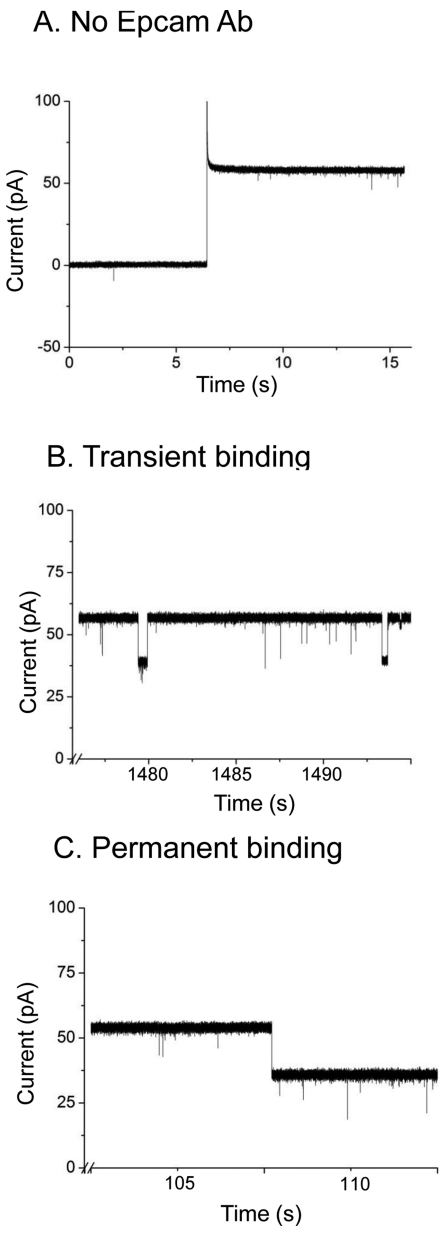

Figure 3. Real-time sensing of EpCAM antibody interactions with EpCAM engineered phi29 connector channels: (A) before addition of EpCAM antibody; (B) transient binding events; (C) permanent binding events.

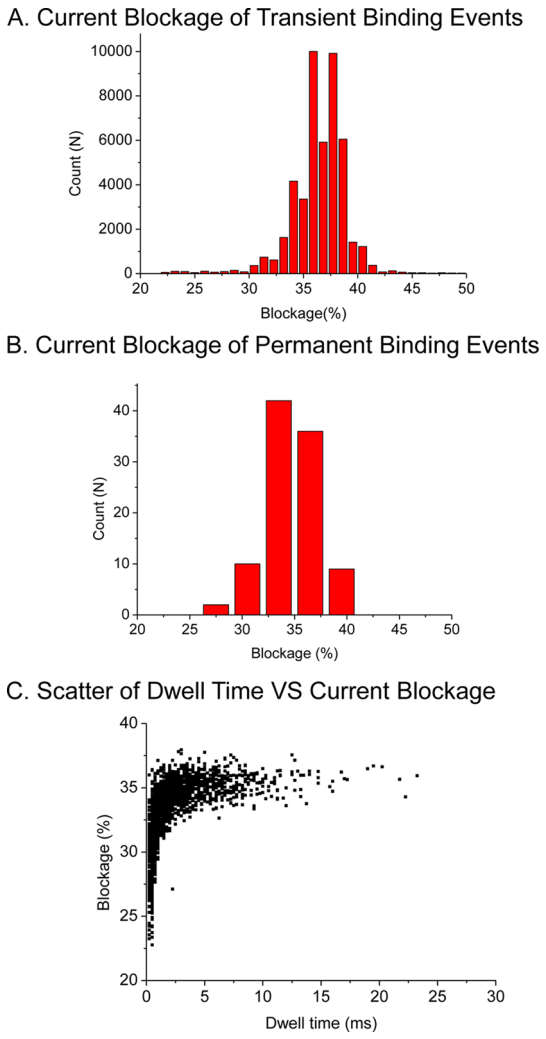

Figure 4. Analysis of current blockage induced by EpCAM probe/antibody interaction; (A) histograms of transient current blockage; (B) histograms of permanent current blockage events; (C) scatter of dwell time *versus* current blockage.

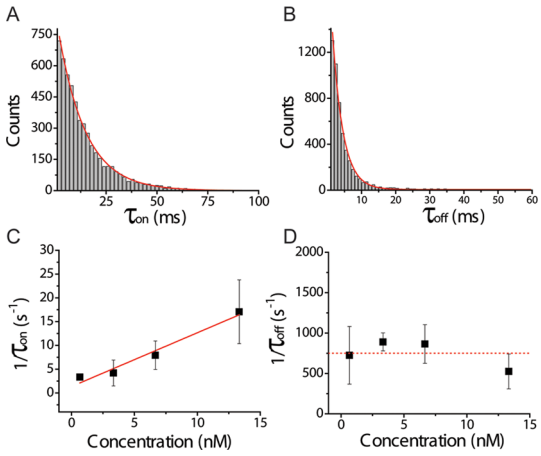

Figure 5. Kinetic studies of EpCAM probe/antibody interaction based on transient dwell time events: (A) event histograms of current time traces τ_{on}, which is the time between two consecutive binding events; (B) event histograms of current time traces τ_{off}, which is the dwell time; (C) Frequency of association as a function of antibody concentration [*P*], which is linear fit to $(1/\overline{\tau}_{on}) = k_{on} \times [P]$, yielding the association rate K_{on}; (D) Frequency of dissociation as a function of antibody concentration [*P*], which is a constant fit to $(1/\overline{\tau}_{off}) = k_{off}$, yielding the dissociation rate K_{off}.

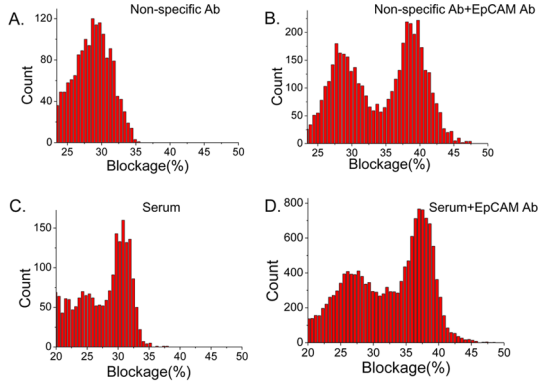

	Non specific peak (%)	EpCAM peak (%)
EpCAM Ab only (Transient)	N/A	36.8±1.8
Non-specific antibody	28.8±2.7	N/A
EpCAM Ab with Non-specific Ab	28.8±2.6	38.9±2.3
Serum only	30.4±1.5	N/A
Epcam Ab in serum	27.6±4.9	37.4±1.9

Figure 6. EpCAM antibody detection in the presence of high concentration of nonspecific antibody and diluted serum: (A) histogram of current blockage events caused by high concentration of nonspecific antibody; (B) histogram of current blockage events caused by high concentration of nonspecific antibody with EpCAM Ab; (C) histogram of current blockage events caused by diluted serum; (D) histogram of current blockage events caused by diluted serum with EpCAM Ab.

The association frequency increased linearly with antibody concentration (Figure 5C). The dissociation rate constant (k_{off}) was determined using the eq $(1/\overline{\tau}_{off}) = k_{off}$. The dissociation frequency was independent of antibody concentration (Figure 5D). On the basis of the two rate constants, the equilibrium dissociation constant (K_d) was determined to be $(6.7 \pm 1.7) \times 10^{-7}$ M.

Selectivity of the EpCAM Probe for EpCAM Antibody in the Presence of Serum and Protein Impurities. In almost all clinical scenarios, a patient's sample will not be highly purified and, most likely, will consist of serum protein and other components (*e.g.*, a blood sample). To investigate how the impurities in the sample affect EpCAM antibody detection and to further push nanopore sensing techniques into the realm of clinical disease diagnosis, we performed the following experiments: (1) EpCAM antibody in the presence of a high concentration of nonspecific antibody; and (2) EpCAM antibody in the presence of diluted serum sample (Figure 6). As the concentration of nonspecific antibodies increased to 10 ng/ul, the current signal caused by nonspecific interaction between the antibody and probe or channel was noted, and the current blockage distribution was determined to be 28.8 ± 2.7%. Under the same buffer conditions containing a high concentration of nonspecific antibody, we increased the

EpCAM concentration to 4 ng/ul and noted another blockage peak, centered at 38.9 ± 2.3%. The position of this new blockage peak was consistent with the previous blockage distribution of EpCAM antibody using the same buffer without nonspecific antibody, indicating that this new blockage peak was caused by EpCAM interaction with the probe.

Serum sample is commonly used in clinical diagnosis. However, most diagnostic studies using nanopore techniques, particulally protein nanopore, have not been conducted in the presence of serum due to the fragile nature of the lipid bilayer, which greatly impedes the pace of applying the nanopore technique for clinical use. Here, we used 100-fold diluted serum with an electrolyte buffer that can maintain its stability for at least one hour. We first tested the noise level caused by impurity in the diluted sample in the presence of diluted serum only. The current blockage distribution was 30.4 ± 1.5%. As the concentration of EpCAM antibody increased to 4 ng/μL, a new blockage peak was noted centered on 37.4 ± 1.9%, which corresponds to the previous EpCAM antibody blockage distribution. This data demonstrates that phi29 nanopore channels are capable of detecting individual molecular species in a complex mixture and can discriminate the signal from background events that are present due to the serum component.

DISCUSSION

The first step for detection of proteins or small molecules is to capture the analyte and gather evidence, such as fingerprints. Many sensing, detection, and diagostic techniques, such as biotin/streptavidin interactions, and microarray-based technologies, have been well developed, but also have a disadvantage: it is not possible to detect a single substrate molecule, regardless of the strength of the antibody affinity. In addition, the background noise will override the specific signal from the antigen/antibody complex at very low concentrations. Recent nanopore studies have detected single protein molecules and distinguished them from the other molecules using engineered specific receptor.[44−46] Compared to conventional protein detection methods, nanopore-based technology has the advantage of label-free, real-time sensing of individual molecules and in the presence of contaminants, all at a relatively low cost.

For the kinetic and thermodynamic studies of macromolecular interactions, nanopore offers several advantages over traditional methods, such as surface Plasmon resonance (SPR) and capillary electrophoresis (CE). For example, steric hindrance due to crowding of the binding sites occurs on the surface of an SPR chip, but does not occur in the nanopore setup.[47] Moreover, the molecular flow rate may interfere with the accuracy of the measurement in SPR and CE. For example, an analyte can rebind to the surface of a chip if the flow rate is too slow in SPR, and this can complicate the kinetic analysis.[47]

EpCAM is a transmembrane glycoprotein, which is highly overexpressed on many cancers. Its ectodomains can be released at levels ranging from 2 to 78 ng/mL into sera of cancer patients.[48] Studies have shown that the expression of EpCAM depends on many factors, such as tumor type, disease stage, tumor microenvironment and host antitumor immunity.[49] In this study, we incorporated an EpCAM peptide into the phi29 connector channel. A linker with 6-glycines was included between the gp-10 connector and the EpCAM peptide probe to provide end flexibility. EpCAM antibody binding was then detected at nanomolar concentrations using single-channel conduction assays. The distinctive current signatures enabled us to analyze the docking and undocking kinetics of antibody-probe interactions and determine the K_d. However, one critical problem limits the application of nanopores for kinetic studies of single molecules: it is time-consuming to study high-affinity interactions. For example, if the ligand remains bound to the receptor for several minutes, several hours may be needed to acquire enough unbinding events. In our study, we observed two classes of current blockage signals: permanent binding and transient binding. For transient blockage events, dwell time lasts tens of milliseconds, suggesting weak interactions between EpCAM antibody and the probe. Therefore, in the kinetic assessment, we based our analysis on the transient events data, which may account for the relatively high K_d (10^{-7} M) compared with the typical K_d of EpCAM-antibody interactions (10^{-8} to 10^{-11} M). Here, the modification on the C-terminal end of phi29 connector channel did not change the conductance and channel size compared with C-his connector channel (Figure 2C). The channel has a diameter of 3.6 nm at the narrow end (N-terminal) and 6 nm at the wide end (C-terminal). Our small peptide antigen was fused to the wide end (C-terminal). Fusing the small peptide antigen to the wide end did not change the conductance of the channel, since conductance is determined by the narrowest end, which was not affected by the C-terminal conjugation with a peptide that sticks out.

Most recent research on applying nanopore techniques for sensing and detection has been performed under ideal conditions using only pure analytes in the presence of the detection system. However, in the majority of clinical samples, the trace analyte is always present in combination with a large proportion of impurities or in serum. To further test the detection capability of this engineered phi29 channel and push nanopore techniques for clinical utilization, we performed the EpCAM antibody detection in the presence of either high concentration nonspecific antibody or diluted serum. We showed that the EpCAM antibody can be distinguished from the background events

present as either nonspecific antibody or serum components.

CONCLUSIONS

Our results demonstrate the feasibility of reengineering the phi29 connector channel for sensing probe−antibody interactions in real-time using single channel conduction assays. The K_d of EpCAM has been calculated from the docking and undocking kinetics of Ab-probe interactions. The signal of EpCAM antibody can be discriminated from the background events in the presence of nonspecific antibody or serum. Our novel findings will inspire future studies to construct more sophisticated connector sensor systems capable of recognizing multiple analytes from ions, small molecules, peptides and small proteins.

EXPERIMENTAL METHODS

Materials. The phospholipid 1,2-diphytanoyl-*sn*-glycerol-3-phosphocholine (DPhPC) was purchased from Avanti Polar Lipids, Inc. Organic solvents (*n*-decane and chloroform) were obtained from Fisher Scientific, Inc. and TEDIA, Inc., respectively. The EpCAM antibody was purchased from Abcam. All other reagents, if not specified, were purchased from Sigma-Aldrich, Inc.

Serum Sample Preparation. Male athymic NCr nude mice between 6 and 8 weeks of age were acquired from Taconic (Hudson, NY) and kept in an animal house with 12 h of light and dark cycles. Food and water was given *ad libitum*. Blood serum was collected from vena cava and allowed to clot for 30 min at room temperature. The clotted material was removed by centrifugation at 2000 rpm for 10 min in a refrigerated centrifuge. Hemolytic material was not observed. The sera obtained from the blood samples were frozen immediately without any further treatment in liquid nitrogen and stored at −80 °C until further use.

Cloning and Purification of the Engineered EpCAM Phi29 Connector Protein. The construction of the plasmid containing the gp-10 gene and the expression and purification of the phi29 connector have been reported previously.[20,22] The new plasmid was constructed first by introducing an EpCAM probe (ELKHKAREKPYDSKSLRT) to the C-terminal of the connector channel, just downstream of gp-10 gene; a His tag was inserted into the N-terminal for purification. The newly constructed clone was transformed into HMS174 (DE3) *Escherichia coli* bacteria. The successfully transformed bacteria were cultured in 10 mL Luria−Bertani medium overnight at 37 °C. These cultured bacteria were transferred to 500 mL of fresh LB medium. When OD_{600} reached 0.5−0.6, 0.5 mM, IPTG was added to the cultured medium to induce protein expression. The bacteria were collected after 3 h, postcentrifugation induction. A French press was used to lyse the bacterial wall, and the protein and other components were differentiated by centrifugation.

An Ni-NTA His bind resin with a His tag was applied to purify the mutant protein. Briefly, 2 mL of regenerated His resin was packed into a column. The supernatant differentiated by centrifugation was loaded into the column. The column was then washed with washing buffer to remove any contaminant proteins. The His-tagged mutated gp10 protein was eluted using elution buffer that contained 500 mM imidazole.

Preparation of Lipid Vesicles Containing EpCAM Engineered Connector Channels. The incorporation of connectors into liposomes has been reported previously.[14] Briefly, 1 mL of 1 mg/mL DPhPC in chloroform was poured in a round-bottomed flask. The chloroform in DPhPC lipid was removed under vacuum. Then, the lipid film that formed was rehydrated with EpCAM engineered connector channel buffer, which contained 1 M NaCl, 10 mM Tris/pH7.9, and 250 mM sucrose to bud off vesicles into the solution. The unilammellar lipid vesicles were generated by passing the lipid solution through a 400 nm polycarbonate membrane filter.

Incorporation of the Connector Channel into a Planar Bilayer Lipid Membrane. The method of inserting the connector with reconstituted liposomes into a lipid bilayer has been reported previously.[14] Briefly, a Teflon film partition (aperture 200 μm in diameter) was used to separate a bilayer lipid membrane chamber (BLM) into *cis* and *trans*-compartments. The aperture was painted two times with 0.5 μL of 3% (w/v) DPhPC *n*-decane solution, and the two compartments were filled with conducting buffer (0.2 M NaCl, 1 mM HEPES, pH 7.4). After the formation of the lipid bilayer on the aperture, the lipid/connector complexes were added to the chamber and allowed to fuse with the planar lipid bilayer.

Single Channel Conduction Assays for Each Membrane Inserted Connector Channels. A pair of Ag/AgCl electrodes was connected directly into the *cis* and *trans*-compartments to measure the current traces across the lipid bilayer membrane. The current trace was recorded using an Axopatch 200B patch clamp amplifier coupled with the Axon DigiData 1322A analog-digital converter (Axon Instruments) or the BLM workstation (Warner Instruments). All voltages reported were those of the *trans*-compartment. Data was low band-pass filtered at a frequency of 1 kHz, and acquired at a sampling frequency of 10−100 kHz. The Patch clamp 9.1 software (Axon Instruments) was used to collect the data, and the software Origin Pro 8.0 was used to analyze all the data.

All antibody binding experiments were conducted under 0.2 M NaCl, 1 mM HEPES, pH 7.4 buffer. EpCAM antibody was added only after the definite insertion of EpCAM engineered connector channels in the lipid bilayer membrane. For selectivity of the EpCAM connector channel study, mouse serum was diluted to 100-fold using the electrolyte buffer; 10 ng/μL of nonspecific antibody was premixed with the buffer. Then EpCAM antibody was added only after the addition of EpCAM engineered connector channels. The current traces were recorded over a period of 1 to 2 h, and all the experiments were repeated at least three times.

Conflict of Interest: The authors declare the following competing financial interest(s): P. Guo is a co-founder of Kylin Therapeutics, Inc., and Biomotor and Nucleic Acid Nanotechnology Development Corp. Ltd.

Acknowledgment. We thank YingYing Guo for the preparation of the phi29 connector channel pdb file. Research was supported by the NIH grant EB012135 (P.G.). The content is solely the responsibility of the authors and does not necessarily represent the official views of NIH, NIBIB, or NIGMS. Funding to Peixuan Guo's Endowed Chair in Nanobiotechnology position is by the William Farish Endowment Fund.

REFERENCES AND NOTES

1. Neher, E.; Stevens, C. F. Conductance Fluctuations and Ionic Pores in Membranes. *Annu. Rev. Biophys. Bioeng.* **1977**, *6*, 345–381.
2. Doyle, D. A.; Morais, C. J.; Pfuetzner, R. A.; Kuo, A.; Gulbis, J. M.; Cohen, S. L.; Chait, B. T.; MacKinnon, R. The Structure of the Potassium Channel: Molecular Basis of K^+ Conduction and Selectivity. *Science* **1998**, *280*, 69–77.
3. Hanson, P. I.; Whiteheart, S. W. AAA+ Proteins: Have Engine, Will Work. *Nat. Rev. Mol. Cell. Biol.* **2005**, *6*, 519–529.
4. Zhao, Z.; Khisamutdinov, E.; Schwartz, C.; Guo, P. Mechanism of One-Way Traffic of Hexameric Phi29 DNA Packaging Motor With Four Electropositive Relaying Layers Facilitating Anti-Parallel Revolution. *ACS Nano* **2013**, *7*, 4082–4092.

5. Schwartz, C.; De Donatis, G. M.; Fang, H.; Guo, P. The ATPase of the Phi29 DNA-Packaging Motor Is a Member of the Hexameric AAA+ Superfamily. *Virology* **2013**, *443*, 20–27.
6. Guo, P. X.; Lee, T. J. Viral Nanomotors for Packaging of DsDNA and DsRNA. *Mol. Microbiol.* **2007**, *64*, 886–903.
7. Sun, S.; Rao, V. B.; Rossmann, M. G. Genome Packaging in Viruses. *Curr. Opin. Struct. Biol.* **2010**, *20*, 114–120.
8. Zhang, F.; Lemieux, S.; Wu, X.; St.-Arnaud, S.; McMurray, C. T.; Major, F.; Anderson, D. Function of Hexameric RNA in Packaging of Bacteriophage Phi29 DNA *in Vitro*. *Mol. Cell* **1998**, *2*, 141–147.
9. Guo, P.; Erickson, S.; Anderson, D. A Small Viral RNA Is Required for *in Vitro* Packaging of Bacteriophage Phi29 DNA. *Science* **1987**, *236*, 690–694.
10. Guo, P.; Zhang, C.; Chen, C.; Trottier, M.; Garver, K. Inter-RNA Interaction of Phage Phi29 PRNA to Form a Hexameric Complex for Viral DNA Transportation. *Mol. Cell* **1998**, *2*, 149–155.
11. Shu, D.; Zhang, H.; Jin, J.; Guo, P. Counting of Six PRNAs of Phi29 DNA-Packaging Motor With Customized Single Molecule Dual-View System. *EMBO J.* **2007**, *26*, 527–537.
12. Simpson, A. A.; Leiman, P. G.; Tao, Y.; He, Y.; Badasso, M. O.; Jardine, P. J.; Anderson, D. L.; Rossman, M. G. Structure Determination of the Head-Tail Connector of Bacteriophage Phi29. *Acta Crystallogr.* **2001**, *D57*, 1260–1269.
13. Guasch, A.; Pous, J.; Ibarra, B.; Gomis-Ruth, F. X.; Valpuesta, J. M.; Sousa, N.; Carrascosa, J. L.; Coll, M. Detailed Architecture of a DNA Translocating Machine: the High-Resolution Structure of the Bacteriophage Phi29 Connector Particle. *J. Mol. Biol.* **2002**, *315*, 663–676.
14. Wendell, D.; Jing, P.; Geng, J.; Subramaniam, V.; Lee, T. J.; Montemagno, C.; Guo, P. Translocation of Double-Stranded DNA through Membrane-Adapted Phi29 Motor Protein Nanopores. *Nat. Nanotechnol.* **2009**, *4*, 765–772.
15. Jing, P.; Haque, F.; Vonderheide, A.; Montemagno, C.; Guo, P. Robust Properties of Membrane-Embedded Connector Channel of Bacterial Virus Phi29 DNA Packaging Motor. *Mol. BioSyst.* **2010**, *6*, 1844–1852.
16. Jing, P.; Haque, F.; Shu, D.; Montemagno, C.; Guo, P. One-Way Traffic of a Viral Motor Channel for Double-Stranded DNA Translocation. *Nano Lett.* **2010**, *10*, 3620–3627.
17. Geng, J.; Fang, H.; Haque, F.; Zhang, L.; Guo, P. Three Reversible and Controllable Discrete Steps of Channel Gating of a Viral DNA Packaging Motor. *Biomaterials* **2011**, *32*, 8234–8242.
18. Geng, J.; Shaoying, W.; Huaming, F.; Peixuan, G. Channel Size Conversion of Phi29 DNA-Packaging Nanomotor for Discrimination of Single- and Double-Stranded DNA and RNA. *ACS Nano* **2013**, *7* (4), 3315–3323.
19. Haque, F.; Lunn, J.; Fang, H.; Smithrud, D.; Guo, P. Real-Time Sensing and Discrimination of Single Chemicals Using the Channel of Phi29 DNA Packaging Nanomotor. *ACS Nano* **2012**, *6*, 3251–3261.
20. Ibanez, C.; Garcia, J. A.; Carrascosa, J. L.; Salas, M. Overproduction and Purification of the Connector Protein of *Bacillus subtilis* Phage Φ29. *Nucleic Acids Res.* **1984**, *12*, 2351–2365.
21. Robinson, M. A.; Wood, J. P.; Capaldi, S. A.; Baron, A. J.; Gell, C.; Smith, D. A.; Stonehouse, N. J. Affinity of Molecular Interactions in the Bacteriophage Phi29 DNA Packaging Motor. *Nucleic Acids Res.* **2006**, *34*, 2698–2709.
22. Guo, Y.; Blocker, F.; Xiao, F.; Guo, P. Construction and 3-D Computer Modeling of Connector Arrays with Tetragonal to Decagonal Transition Induced by PRNA of Phi29 DNA-Packaging Motor. *J. Nanosci. Nanotechnol.* **2005**, *5*, 856–863.
23. Xiao, F.; Sun, J.; Coban, O.; Schoen, P.; Wang, J. C.; Cheng, R. H.; Guo, P. Fabrication of Massive Sheets of Single Layer Patterned Arrays Using Lipid Directed Reengineered Phi29 Motor Dodecamer. *ACS Nano* **2009**, *3*, 100–107.
24. Cai, Y.; Xiao, F.; Guo, P. The Effect of N- or C-Terminal Alterations of the Connector of Bacteriophage Phi29 DNA Packaging Motor on Procapsid Assembly, PRNA Binding, and DNA Packaging. *Nanomedicine* **2008**, *4*, 8–18.
25. Haque, F.; Li, J.; Wu, H.-C.; Liang, X.-J.; Guo, P. Solid-State and Biological Nanopore for Real-Time Sensing of Single Chemical and Sequencing of DNA. *Nano Today* **2013**, *8*, 56–74.
26. Branton, D.; Deamer, D. W.; Marziali, A.; Bayley, H.; Benner, S. A.; Butler, T.; Di, V. M.; Garaj, S.; Hibbs, A.; Huang, X.; *et al.* The Potential and Challenges of Nanopore Sequencing. *Nat. Biotechnol.* **2008**, *26*, 1146–1153.
27. Venkatesan, B. M.; Bashir, R. Nanopore Sensors for Nucleic Acid Analysis. *Nat. Nanotechnol.* **2011**, *6*, 615–624.
28. Healy, K. Nanopore-Based Single-Molecule DNA Analysis. *Nanomedicine* **2007**, *2*, 459–481.
29. Majd, S.; Yusko, E. C.; Billeh, Y. N.; Macrae, M. X.; Yang, J.; Mayer, M. Applications of Biological Pores in Nanomedicine, Sensing, and Nanoelectronics. *Curr. Opin. Biotechnol.* **2010**, *21*, 439–476.
30. Iqbal, S. M.; Bashir, R. *Nanopores: Sensing and Fundamental Biological Interactions*; Springer London, Limited: London, 2011.
31. Bayley, H.; Cremer, P. S. Stochastic Sensors Inspired by Biology. *Nature* **2001**, *413*, 226–230.
32. Raj, A.; van, O. A. Single-Molecule Approaches to Stochastic Gene Expression. *Annu. Rev. Biophys.* **2009**, *38*, 255–270.
33. Perkins, T. J.; Swain, P. S. Strategies for Cellular Decision-Making. *Mol. Syst. Biol.* **2009**, *5*, 326.
34. Bayley, H.; Martin, C. R. Resistive-Pulse Sensing-From Microbes to Molecules. *Chem. Rev.* **2000**, *100*, 2575–2594.
35. Sauer-Budge, A. F.; Nyamwanda, J. A.; Lubensky, D. K.; Branton, D. Unzipping Kinetics of Double-Stranded DNA in a Nanopore. *Phys. Rev. Lett.* **2003**, *90*, 238101.
36. Balzar, M.; Winter, M. J.; de Boer, C. J.; Litvinov, S. V. The Biology of the 17−1A Antigen (Ep-CAM). *J. Mol. Med. (Heidelberg, Ger.)* **1999**, *77*, 699–712.
37. de Boer, C. J.; van Krieken, J. H.; Janssen-van Rhijn, C. M.; Litvinov, S. V. Expression of Ep-CAM in Normal, Regenerating, Metaplastic, and Neoplastic Liver. *J. Pathol.* **1999**, *188*, 201–206.
38. High, A. S.; Robinson, P. A.; Klein, C. E. Increased Expression of a 38kd Cell-Surface Glycoprotein MH99 (KS 1/4) in Oral Mucosal Dysplasias. *J. Oral Pathol. Med.* **1996**, *25*, 10–13.
39. Pauli, C.; Munz, M.; Kieu, C.; Mack, B.; Breinl, P.; Wollenberg, B.; Lang, S.; Zeidler, R.; Gires, O. Tumor-Specific Glycosylation of the Carcinoma-Associated Epithelial Cell Adhesion Molecule EpCAM in Head and Neck Carcinomas. *Cancer Lett.* **2003**, *193*, 25–32.
40. Poczatek, R. B.; Myers, R. B.; Manne, U.; Oelschlager, D. K.; Weiss, H. L.; Bostwick, D. G.; Grizzle, W. E. Ep-Cam Levels in Prostatic Adenocarcinoma and Prostatic Intraepithelial Neoplasia. *J. Urol.* **1999**, *162*, 1462–1466.
41. Shetye, J.; Christensson, B.; Rubio, C.; Rodensjo, M.; Biberfeld, P.; Mellstedt, H. The Tumor-Associated Antigens BR55−2, GA73−3 and GICA 19−9 in Normal and Corresponding Neoplastic Human Tissues, Especially Gastrointestinal Tissues. *Anticancer Res.* **1989**, *9*, 395–404.
42. Spizzo, G.; Gastl, G.; Wolf, D.; Gunsilius, E.; Steurer, M.; Fong, D.; Amberger, A.; Margreiter, R.; Obrist, P. Correlation of COX-2 and Ep-CAM Overexpression in Human Invasive Breast Cancer and Its Impact on Survival. *Br. J. Cancer* **2003**, *88*, 574–578.
43. Sarma, V. R.; Silverton, E. W.; Davies, D. R.; Terry, W. D. The Three-Dimensional Structure at 6 Å Resolution of a Human Gamma Gl Immunoglobulin Molecule. *J. Biol. Chem.* **1971**, *246*, 3753–3759.
44. Rotem, D.; Jayasinghe, L.; Salichou, M.; Bayley, H. Protein Detection by Nanopores Equipped with Aptamers. *J. Am. Chem. Soc.* **2012**, *134*, 2781–2787.
45. Li, W.; Bell, N. A.; Hernandez-Ainsa, S.; Thacker, V. V.; Thackray, A. M.; Bujdoso, R.; Keyser, U. F. Single Protein Molecule Detection by Glass Nanopores. *ACS Nano* **2013**, *7* (5), 4129–4134.
46. Wei, R.; Gatterdam, V.; Wieneke, R.; Tampe, R.; Rant, U. Stochastic Sensing of Proteins with Receptor-Modified Solid-State Nanopores. *Nat. Nanotechnol.* **2012**, *7*, 257–263.

47. Myszka, D. G. Kinetic Analysis of Macromolecular Interactions Using Surface Plasmon Resonance Biosensors. *Curr. Opin. Biotechnol.* **1997**, *8*, 50–57.
48. Abe, H.; Kuroki, M.; Imakiire, T.; Yamauchi, Y.; Yamada, H.; Arakawa, F.; Kuroki, M. Preparation of Recombinant MK-1/Ep-CAM and Establishment of an ELISA System for Determining Soluble MK-1/Ep-CAM Levels in Sera of Cancer Patients. *J. Immunol. Methods* **2002**, *270*, 227–233.
49. Sterzynska, K.; Kempisty, B.; Zawierucha, P.; Zabel, M. Analysis of the Specificity and Selectivity of Anti-EpCAM Antibodies in Breast Cancer Cell Lines. *Folia Histochem. Cytobiol.* **2012**, *50*, 534–541.